NAR Molecular Medicine, 2025, **2**, ugaf007
https://doi.org/10.1093/narmme/ugaf007
Advance access publication date: 19 March 2025
Standard Article

SRSF6 and SRSF1 coordinately enhance the inclusion of human *MUSK* exon 10 to generate a Wnt-sensitive MuSK isoform

Farhana Nasrin [1,2,†], Preeti Nagar [1,†], Md Rafikul Islam [1,†], Shabiha Afroj Heeamoni [1], Md Mahbub Hasan [1], Kinji Ohno [2,3], Mohammad Alinoor Rahman [1,4,*]

[1]Department of Biochemistry and Molecular Biology, University of Arkansas for Medical Sciences, Little Rock, AR 72205, United States
[2]Division of Neurogenetics, Center for Neurological Diseases and Cancer, Nagoya University Graduate School of Medicine, Nagoya, 4668550 Aichi, Japan
[3]Graduate School of Nutritional Sciences, Nagoya University of Arts and Sciences, Nisshin, 4700196 Aichi, Japan
[4]Winthrop P. Rockefeller Cancer Institute, University of Arkansas for Medical Sciences, Little Rock, AR 72205, USA

[*]To whom correspondence should be addressed. Email: marahman@uams.edu
[†]The first three authors should be regarded as Joint First Authors.

Abstract

Alternative splicing in genes associated with neuromuscular junction (NMJ) often compromises neuromuscular signal transmission and provokes pathological consequences. Muscle-specific receptor tyrosine kinase (MuSK) is an essential molecule in the NMJ. *MUSK* exon 10 encodes an important part of the frizzled-like cysteine-rich domain, which is necessary for Wnt-mediated acetylcholine receptors clustering at NMJ. *MUSK* exon 10 is alternatively spliced in humans but not in mice. We reported that humans acquired a unique exonic splicing silencer in exon 10 compared to mice, which promotes exon skipping coordinated by hnRNP C, YB-1, and hnRNP L. Here, we have dissected the underlying mechanisms of exon inclusion. We precisely characterized the exonic splicing enhancer (ESE) elements and determined the functional motifs. We demonstrated that SRSF6 and SRSF1 coordinately enhance exon inclusion through multiple functional motifs in the ESE. Remarkably, SRSF6 exerts a stronger effect than SRSF1, and SRSF6 alone can compensate the function of SRSF1. Interestingly, differentiated muscle reduces the expression of splicing suppressors, rather than enhancers, to generate a functional Wnt-sensitive MuSK isoform to promote neuromuscular signal transmission. Finally, we developed splice-switching antisense oligonucleotides, which could be used to selectively modulate the expression of *MUSK* isoforms toward a beneficial outcome for therapeutic intervention.

Graphical abstract

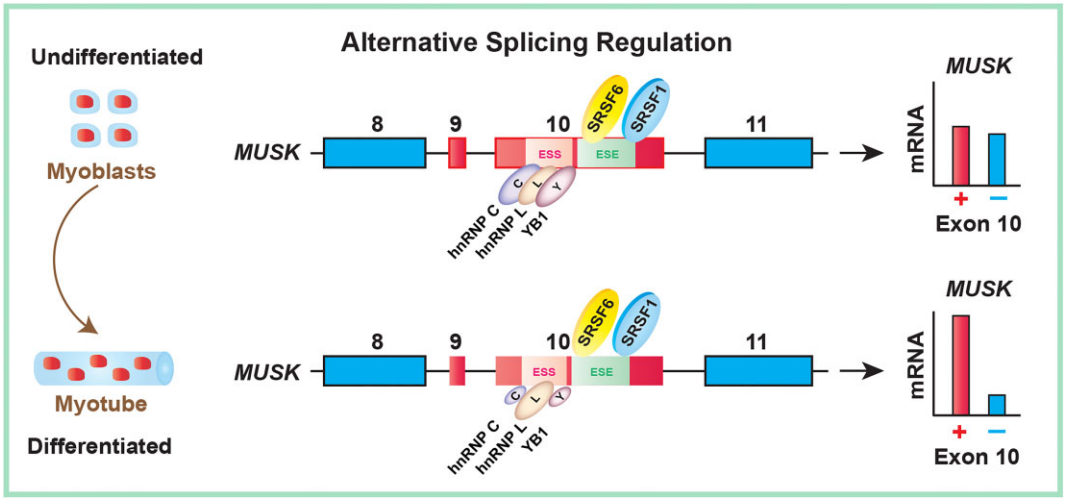

Received: January 2, 2025. **Revised:** March 7, 2025. **Editorial Decision:** March 17, 2025. **Accepted:** March 18, 2025

Introduction

Alternative splicing (AS) can encode multiple protein isoforms from a single gene to promote proteome diversity [1–5]. AS evolved as a key control point of gene expression. Regulation of AS is cooperatively orchestrated with the dynamic choreography of *cis*-elements in the RNA comprised of exonic/intronic splicing enhancers (ESEs/ISEs) or silencers (ESSs/ISSs) and cognate *trans*-acting splicing factors [1, 2]. This is further regulated in a tissue-specific and developmental stage-specific manner to support rapidly changing biological processes. The dynamic assembly of ribonucleoprotein complexes (RNPs) is coordinated with strict fidelity, which is critical to ensure that the correct *trans*-acting splicing factors are escorted in the correct RNA in the right cell at the right time to ensure rapidly changing cellular function.

Muscle-specific receptor tyrosine kinase (MuSK) is an important protein constituting the key molecular architecture of the neuromuscular junction (NMJ), which plays a pivotal role in neuromuscular signal transmission to enable proper muscle contraction [6–9]. MuSK obtains a complex structure to respond to its ligands. The ectodomain of MuSK comprises three immunoglobulin (Ig)-like domains (Ig-1, Ig-2, and Ig-3) and a single frizzled-like cysteine-rich domain (Fz-CRD) [6–9], encoded by exons 10 and 11 (Fig. 1A and B). The first Ig-like domain (Ig1) of MuSK is important for agrin to activate MuSK phosphorylation via LRP4 [10]. In contrast, the Fz-CRD domain is required for Wnt proteins to activate MuSK, which requires LRP4 but not agrin [9, 10]. In humans but not in mice, *MUSK* exon 10, encoding six out of ten essential cysteines residues of Fz-CRD, is alternatively skipped (Fig. 1A and B), therefore likely to generate a Wnt-insensitive MuSK isoform [9, 11, 12]. We previously reported that hnRNP C, YB-1, and hnRNP L coordinately promote the skipping of *MUSK* exon 10 by binding to an exonic splicing silencer (ESS) unique to humans [9]. In this communication, we have investigated the underlying mechanisms that drive the inclusion of *MUSK* exon 10 to generate a Wnt-sensitive MuSK isoform, which is essential for NMJ signal transmission.

Serine/arginine-rich splicing factor 1 (SRSF1) is a member of the serine and arginine-rich protein (SR) family [13]. It is a ubiquitously expressed protein and functions as a splicing factor in both constitutive and AS [14]. SRSF1 also plays an important role in nonsense-mediated messenger RNA (mRNA) decay (NMD) [15–17], mRNA transport [18–20], and protein translation [21]. Furthermore, *SRSF1* is reported to be a proto-oncogene [22–24]. SRSF6 is another member of the SR protein family [13]. It is ubiquitously expressed and reported to regulate AS, translation, wound healing, and tissue homeostasis [5, 25–28]. SRSF6 also functions as an oncoprotein to regulate the proliferation and survival of lung and colon cancers [5, 29]. It was shown that upregulation or downregulation of the expression of SRSF6 changed the splicing of several tumor suppressors and oncogenes, which subsequently contributed to producing oncogenic isoforms [29].

In this manuscript, we show that SRSF6 and SRSF1 coordinately enhance recognition of *MUSK* exon 10 by binding to an exonic splicing enhancer (ESE) to generate a Wnt-sensitive MuSK isoform. Remarkably, SRSF6 has a more prominent effect than SRSF1, and SRSF6 is able to compensate for exon inclusion activity even in the absence of SRSF1. We also revealed that differentiated muscle reduces the expression of splicing suppressors, rather than enhancers, to upregulate exon 10 inclusion and the expression of a Wnt-sensitive MuSK isoform. Finally, we developed antisense oligonucleotides (ASOs) to selectively manipulate the expression of *MUSK* isoforms with or without exon 10 as a proof of concept for any future therapeutic targeting.

Materials and methods

Cell culture and transfection

HeLa cells (ATCC) were cultured in DMEM media (Sigma–Aldrich) with 10% fetal bovine serum (FBS, Sigma–Aldrich). Immortalized human myogenic cell line (Hu5/KD3) was a kind gift from Dr. Naohiro Hashimoto (National Center for Geriatrics and Gerontology, Japan) [30–32]. Hu5/KD3 cells were grown in high-glucose (4.5 g/ml) DMEM (hDMEM) media containing 20% FBS and 2% Ultroser G serum substitute (PALL). HeLa cells were transfected with the Lipofectamine 2000 transfection reagent (Thermo Fisher Scientific) according to the manufacturer's instructions.

MUSK minigene for splicing analysis

We cloned human *MUSK* exon 10 and flanking intronic sequences (245 nucleotides of intron 9 and 200 nucleotides of intron 10) in the modified exon-trapping vector, pSPL3 into NotI and PacI sites [9]. Artificial mutations and replacement of individual blocks in block scanning mutagenesis experiments were engineered into the pSPL3 minigenes using the QuikChange site-directed mutagenesis (Agilent). The sequences of primers for constructing the minigenes are shown in Supplementary Table S1.

RT-PCR

Total RNA was extracted 48 h after transfection using Trizol (Invitrogen) and treated with DNase I (Qiagen). Complementary DNA (cDNA) was synthesized using ReverTra Ace reverse transcriptase (Toyobo) and an oligo-dT primer (Invitrogen). Reverse transcription polymerase chain reaction (RT-PCR) was conducted using GoTaq (Promega) Master Mixes. The sequences of primers for RT-PCR are shown in Supplementary Table S2.

RNA affinity purification assay

Biotinylated RNA probes were synthesized using the T7 RiboMAX large-scale RNA production system (Promega). We used 3.0 mM Biotin-14-CTP (Invitrogen) as reported previously [33]. The RNA affinity purification method was slightly modified from the previously described protocol [33]. A biotinylated RNA probe (1.0 nmol) was mixed with HeLa nuclear extract (50 µl) (CilBiotech) in a 500-µl binding buffer [20 mM HEPES, pH 7.8, 150 mM KCl, 0.1 mM EDTA, 1 mM DTT, 1 mM phenylmethylsulfonyl fluoride (PMSF), 0.05% Triton X, 1× Protease Inhibitor Cocktail (Active Motif)]. The mixture was then incubated at 30°C for 6 h with gentle rotation. In the meantime, 50 µl streptavidin-conjugated beads (Streptavidin-sepharose, GE Healthcare) were blocked with 1 ml binding buffer (1:1 mixture) with yeast transfer RNA (tRNA) (0.1 mg/ 100 µl of beads) and 1 ml PBS containing 4% BSA. The mixture was then incubated at 4°C for 1 h with gentle rotation. After washing the beads with 1 ml binding buffer (four times), RNA-bound proteins were eluted in SDS loading buffer at 95°C for 5 min. The purified proteins were fractionated on a 10% sodium dodecyl sulfate (SDS)–polyacrylamide

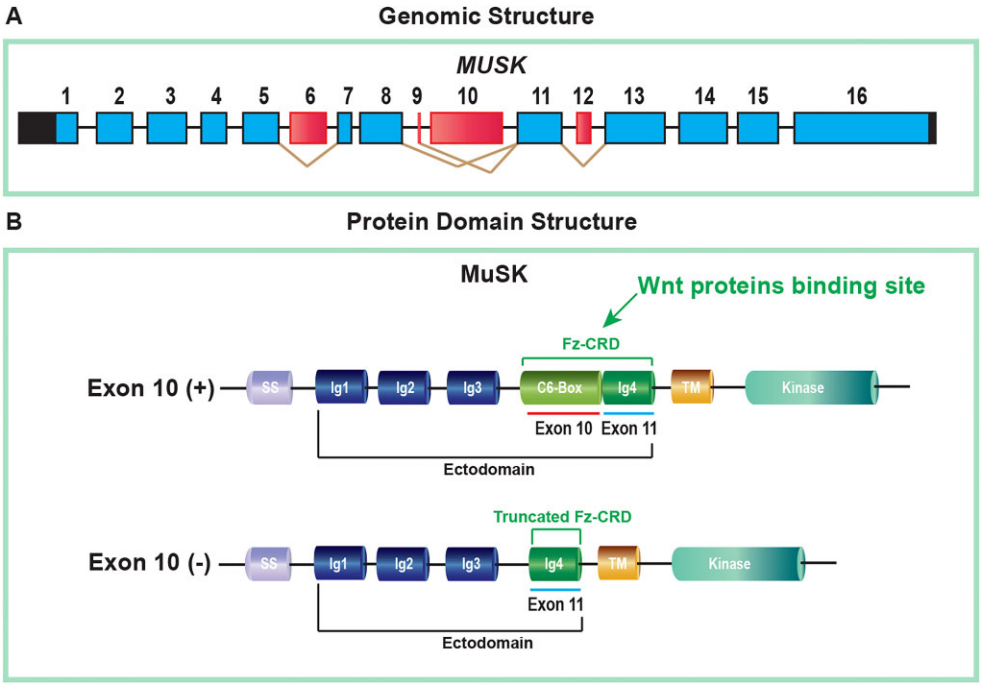

Figure 1. Structural features of human MuSK. (**A**) Genomic structure of *MUSK* gene (not in scale). Constitutive exons are shown in blue boxes, whereas alternative exons are shown in red boxes. Untranslated regions are marked by black boxes, and black lines represent introns. Alternative exon skipping is shown by brown connecting lines. (**B**) Schematics of *MUSK* exon 10 included (+) and excluded (-) protein isoforms (not in scale). Fz-CRD is a Wnt-binding domain, which is important for Wnt-mediated AChRs clustering at the NMJ. Fz-CRD contains 10 highly conserved cysteine residues important for structural folding. Exon 10 encodes for 6 cysteines (C6-Box), and exon 11 encodes for 4 cysteines (Ig4) of Fz-CRD. Fz-CRD, frizzled-like cysteine-rich domain; Ig, immunoglobulin-like domain; SS, signal sequence; TM, transmembrane domain.

gel and processed for Coomassie blue staining or immunoblotting (IB). Excised protein bands from Coomassie blue stained gel were resolved by mass spectrometry as described previously [9, 33].

siRNA knockdown and minigene splicing

We used the following human small interfering RNAs or siRNAs (SIGMA):

- siSRSF6: 5′-GCAGATCCAGGTCTCGATCTT-3′;
- siSRSF1: SASI_Hs01_00115056

We used AllStar Negative Control siRNA (1027281) by Qiagen as control. Cells were plated 24 h before transfection in six-well culture plates (1.5×10^5 cells/well). The transfection reagent included each siRNA duplex at a final concentration of 30 nM, Lipofectamine 2000 transfection reagent (Thermo Fisher Scientific), and 500 ng minigene in 100 µl Opti-MEM medium. The cells were processed 2 days after transfection for RT-PCR and IB analyses.

cDNA expression and minigene splicing

Human SRSF1 and SRSF6 cDNA clones were constructed previously in the Adrian Krainer lab at Cold Spring Harbor Laboratory [17, 34]. Cells were plated 24 h prior to transfection in a six-well culture plate (1.5×10^5 cells/well) and transfected with 500 ng of an expression construct and 500 ng of the minigene using XtremeGENE 9 (Roche) transfection reagent in 100 µl Opti-MEM medium according to manufacturer's instructions. The cells were harvested 2 days after transfection for RT-PCR and IB analyses.

Antisense oligonucleotides-mediated splicing manipulation

We synthesized affinity plus ASOs from Integrated DNA Technologies (IDT) with 2′ modifications on the sugar moiety (locked nucleic acid bases) to prevent RNase H activation. The sequences of ASOs are shown in Supplementary Table S3. ASOs were transfected using Lipofectamine 2000 transfection reagent (Thermo Fisher Scientific) as described before [17]. The cells were processed 2 days after transfection for RT-PCR.

Harvesting cells for immunoblotting

Cells were washed and harvested in PBS with 1× Protease Inhibitor Cocktail. After centrifugation at 2000 × *g* for 5 min, the pellets were resuspended in buffer A [10 mM HEPES-NaOH (pH 7.8), 10 mM KCl, 0.1 mM EDTA, 1 mM dithiothreitol (DTT), 0.5 mM PMSF, 0.1% Nonidet P-40, 1× Protease Inhibitor Cocktail] and incubated on ice for 30 min. Samples were sonicated and centrifuged at 20 000 × *g* for 5 min to remove cell debris. The total cell lysate was analyzed for IB.

Tethered function assay

Tethered function assay was conducted by cotransfection of a reporter minigene and an effector construct. The minigene was designed to carry an MS2 coat protein-binding hairpin site. In contrast, an effector construct (cDNA of SRSF1 or SRSF6) was fused to an MS2 coat protein cDNA. MS2-tagged SRSF1 and SRSF6 cDNAs were constructed previously in the Adrian Krainer lab at Cold Spring Harbor Laboratory [17, 34]. We substituted the bacteriophage MS2 coat protein-binding hairpin RNA sequence (5′-ACATGAGGATCACCCATGT-3′) [33]

for sequences 5′-TGCGGAC-3′, 5′-TGAGGAGG-3′, or 5′-CACGGCC-3′ in *MUSK* exon 10 in the pSPL3-human-*MUSK* minigene using the QuikChange site-directed mutagenesis.

Antibodies

Antibodies used in this study were anti-hnRNP C1/C2 4F4 (SC-32308, Santa Cruz Biotechnology), anti-YB1 (A303-230A, Bethyl Laboratories), anti-hnRNP L (A303-896A, Bethyl Laboratories), anti-SRSF6 (Anti-SRp55, A303-669A, Bethyl Laboratories), anti-SRSF1 (Anti-ASF, A302-052A, Bethyl Laboratories), anti-GAPDH (G9545, Sigma–Aldrich), and anti-T7-tag antibody (T7-KLH 42 1-87, Cold Spring Harbor Laboratory) [17].

Densitometric analysis

RT-PCR and IB images were quantified using the ImageJ (1.54g) software.

Statistical analysis

Statistical calculations were performed using the GraphPad Prism (10.2.3) software.

Results

SRSF6 and SRSF1 bind to the ESE of *MUSK* exon 10

Previously, we identified exonic splicing *cis*-elements responsible for splicing of human *MUSK* exon 10 using a splicing reporter minigene (pSPL3-human-*MUSK*) [9]. We characterized ESS precisely (blocks 5 and 12) (Fig. 2A, lanes 6 and 13). To characterize ESE, we first reconfirmed the activity of ESE by sequential replacement of 20-nucleotide blocks throughout the ESE with 20-nucleotide heterologous sequence (5′-TCAGTATGACTCTCAGTATG-3′), having no splicing activity as described previously [35, 36]. As expected, the replacement of ESE sequences (blocks 6–9) resulted in the loss of exon inclusion activity (Fig. 2A, lanes 7–10). Splicing regulatory *cis*-elements have been reported to function generally by binding to the cognate regulatory proteins [37]. To determine if potential *trans*-acting factors specifically interact with the ESE sequences, binding reactions were performed with a HeLa nuclear extract and a biotinylated RNA probe spanning the entire ESE (ESE-wt) (blocks 6–9, 80 nucleotides) (Fig. 2B). We synthesized a mutant RNA probe as a control, where we introduced artificial mutations in order to decrease the overall ESE activity as demonstrated by *in silico* analysis (ESEfinder 3.0) [38–40] (Fig. 2B and Supplementary Fig. S1). Note that we kept the individual base composition the same between ESE-wt and ESE-mut probes. We performed an RNA affinity purification assay using the RNA probes (Fig. 2C). A Coomassie-stained gel of affinity-purified products showed two distinct bands of ∼55 and ∼30 kD associated with the wild-type ESE RNA probe but not with the mutant probe (Fig. 2D). These two bands were consistently identified in multiple experiments. We excised these two bands from the gel and ran for mass spectrometry (MS). Analyses of the identified peptides by MASCOT revealed the origin of the ∼55 kD band as human SRSF6 (previously termed as SRp55) with a MASCOT protein score of 48, and the ∼30 kD band as human SRSF1 (previously termed as SF2/ASF) with a MASCOT protein score of 63 [13]. There were a few other bands associated with both probes but more prominently with ESE-wt (Fig. 2D), which appeared as common contaminants of MS, such as keratins. We reconfirmed the binding of each factor (SRSF6 and SRSF1) by IB using specific antibodies against SRSF1 and SRSF6, respectively (Fig. 2E).

SRSF6 and SRSF1 enhance the inclusion of human *MUSK* exon 10

We next sought to evaluate the effects of the identified *trans*-factors on the inclusion of *MUSK* exon 10. We first employed siRNA-mediated downregulation of the individual factors (SRSF1 or SRSF6) in HeLa cells. We first confirmed the efficient downregulation of each of the factors by IB (Fig. 3A). Downregulation of either SRSF6 or SRSF1 caused a loss of exon 10 inclusion activity of transfected pSPL3-human-*MUSK* (Fig. 3B, lanes 2 and 3). Downregulation of both *trans*-factors simultaneously exerted a more prominent effect compared to individual effects (Fig. 3B, lane 4 compared to lanes 2 and 3). Our data suggest that SRSF6 and SRSF1 are likely to have additive effects on exon inclusion.

We next set out experiments for cDNA expression of each of the *trans*-factors individually or simultaneously (SRSF6 or/and SRSF1) in HeLa cells. We employed T7-tagged SRSF1 and SRSF6 cDNA constructs. We confirmed the expression of each of the cDNAs by IB using a T7-tag antibody (Fig. 3C). As expected, overexpression of either SRSF6 or SRSF1 induced the inclusion of exon 10 of transfected pSPL3-human-*MUSK* (Fig. 3D, lanes 2 and 3). The most prominent inclusion was observed when two factors were overexpressed simultaneously (Fig. 3D, lane 4 compared to lanes 2 and 3). These results were consistent with the knockdown experiments. Recapitulation of consistent splicing regulatory effects in cDNA overexpression experiments ruled out the possible off-target effects of siRNAs used in knockdown experiments.

SRSF6 can compensate for the splicing activity of SRSF1 for *MUSK* exon 10

We next asked if one of the identified factors is sufficient to compensate for the absence of the other factor or not. To this end, we expressed SRSF6 cDNA in HeLa cells treated with siRNA against SRSF1. To our surprise, SRSF6 could rescue the effect of SRSF1 downregulation on *MUSK* exon 10 inclusion of transfected pSPL3-human-*MUSK* (Fig. 3E, lane 3 compared to lane 2). However, this rescue effect was not observed when SRSF1 cDNA was expressed in HeLa cells treated with siRNA against SRSF6 (Fig. 3E, lane 5 compared to lane 4). Therefore, we can conclude that SRSF6 is essentially the major ESE of exon 10, which functions in cooperation with the additive effect of SRSF1.

Molecular basis of binding and splicing regulation promoted by SRSF6 and SRSF1

To characterize the molecular basis of SRSF6- and SRSF1-mediated ESE activity, we further extended our analysis to characterize precise binding motifs of SRSF6 and SRSF1 in the identified ESE. According to *in vitro* SELEX study, the binding consensus for SRSF6 is T(G/C)CG(T/G)(A/C), whereas the binding consensus for SRSF1 is (G/C)(A/G)(G/C)A(G/C)GA [41]. However, the binding motifs of both SRSF6 and SRSF1 identified by biochemical and mutagenesis analyses always do not strictly match the SELEX consensus and show degeneracy to some extent [14, 26, 27, 42–45]. Considering all preferred-binding motifs, we scanned *MUSK* exon 10

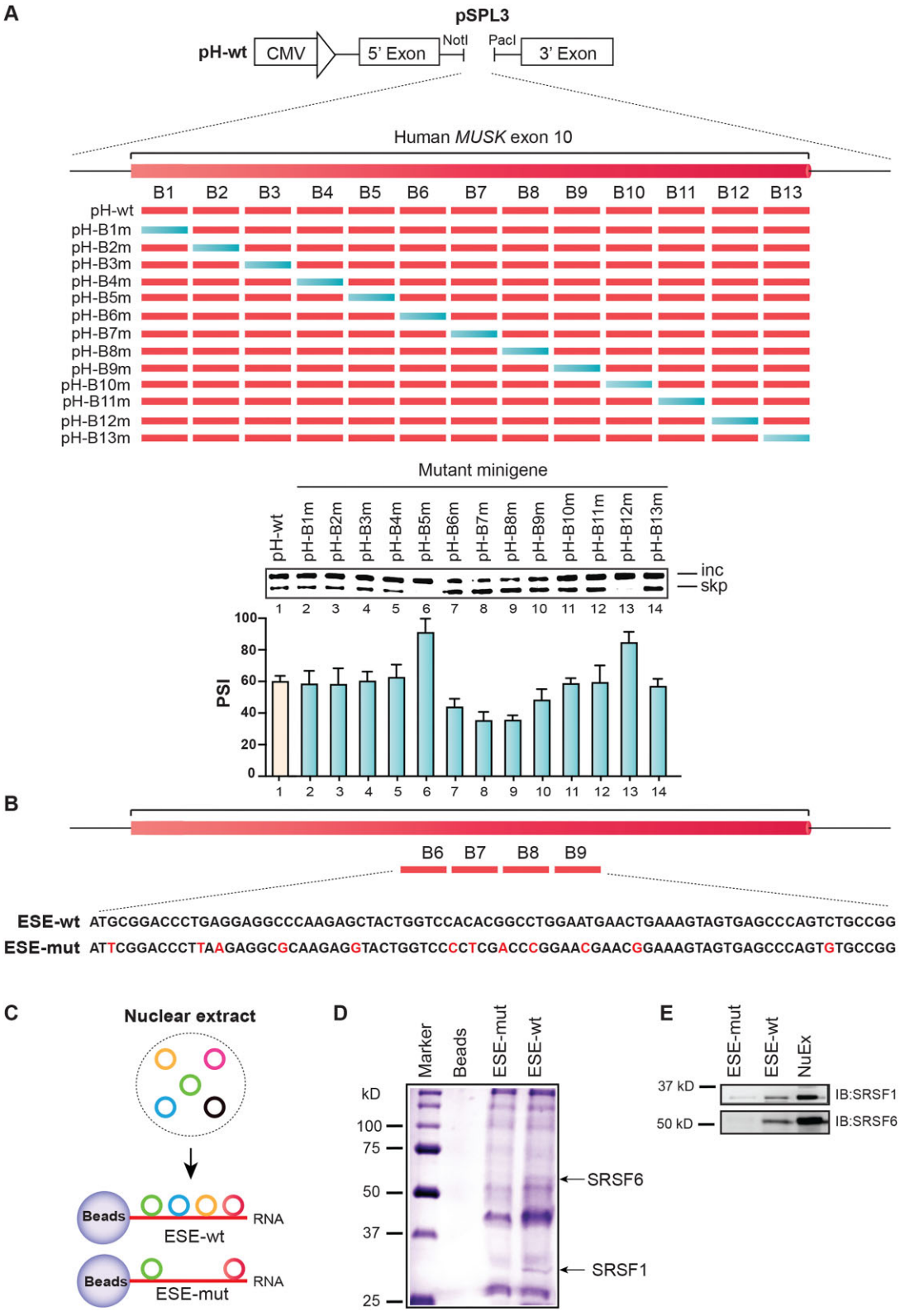

Figure 2. Characterizing ESE elements in *MUSK* exon 10 and identification of cognate RNA-binding proteins. (**A**) Top, schematics of pSPL3-human-*MUSK* minigene (pH-wt) and block-scanning mutagenesis. A long red box denotes *MUSK* exon 10, and black lines denote flanking introns. Each 20-nucleotide block in exon 10 (shown by small red boxes, B1–B13) was substituted with a heterologous sequence of 5′-TCAGTATGACTCTCAGTATG-3′ (shown by blue). Middle, splicing RT-PCR of pH-wt and 13 block-mutant minigenes (B1–B13) in HeLa cells. Bottom, quantification of exon 10 inclusion (percent spliced-in, PSI) is shown by a bar graph (mean ± SD, $n = 3$ biological replicates). (**B**) Sequences of biotinylated ESE RNA probe (spanning blocks B6–B9) carrying wild-type (ESE-wt) or mutated (ESE-mut) sequences. (**C**) Schematics of RNA affinity purification assay. (**D**) Coomassie blue staining of RNA affinity-purified products from HeLa nuclear extract using the indicated biotinylated RNA probes. Two proteins of ~55 and ~30 kDa (arrows) are differentially associated with ESE-wt compared to ESE-mut. Mass spectrometry analysis revealed that the two proteins are human SRSF6 and SRSF1, respectively. (**E**) IB of RNA affinity purified proteins in panel (D) with the indicated antibodies. Inc: exon inclusion; skp: exon skipping; NuEx: nuclear extract.

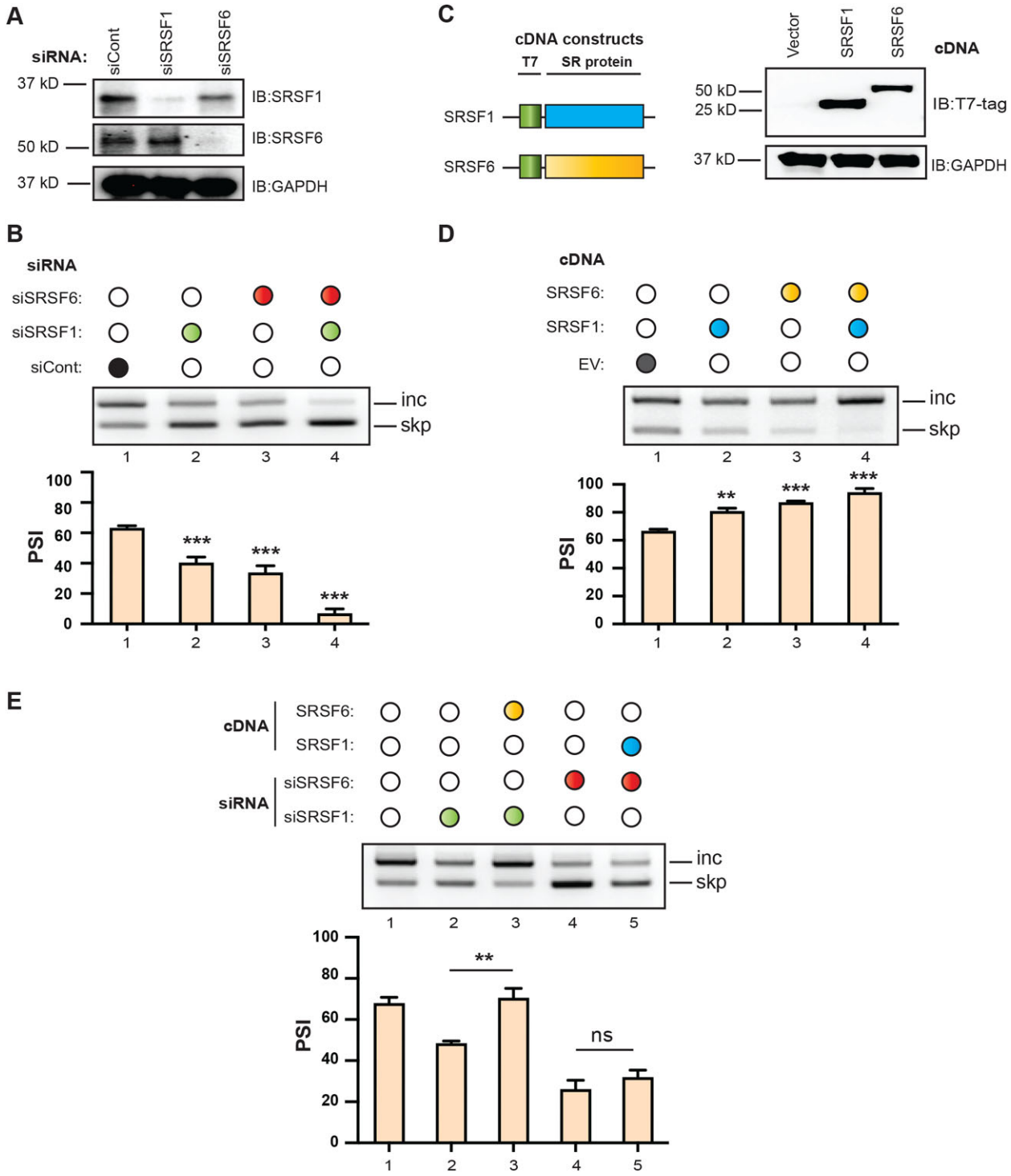

Figure 3. SRSF6 enhances the inclusion of *MUSK* exon 10 in cooperation with SRSF1. (**A**) IB using the indicated antibodies after gene knockdown with siRNA against control (siCont), human SRSF6 (siSRSF6), and human SRSF1 (siSRSF1) in HeLa cells. (**B**) RT-PCR of pSPL3-human-*MUSK* minigene (pH-wt) in HeLa cells treated with the indicated siRNAs. The black circle indicates siCont, the red circle indicates siSRSF6, the green circle indicates siSRSF1, and the white circle indicates blank treatment. Quantification of *MUSK* exon 10 inclusion (PSI) is shown by a bar graph (mean ± SD, $n = 3$ biological replicates) below the gel. (**C**) Schematics of cDNA constructs (left). IB with the indicated antibodies after a T7-tagged cDNA expression encoding human SRSF6 or SRSF1 in HeLa cells (right). (**D**) RT-PCR of pSPL3-human-*MUSK* minigene (pH-wt) in HeLa cells co-transfected with the indicated cDNAs. The yellow circle indicates SRSF6 cDNA, the blue circle indicates SRSF1 cDNA and the white circle indicates blank treatment. Quantification of *MUSK* exon 10 inclusion (PSI) is shown by a bar graph (mean ± SD, $n = 3$ biological replicates) below the gel. (**E**) RT-PCR of pSPL3-human-*MUSK* minigene (pH-wt) in HeLa cells treated with the indicated siRNA and/or cDNA. Circles indicate the same as described in panels (B) and (D). Quantification of *MUSK* exon 10 inclusion (PSI) is shown by a bar graph (mean ± SD, $n = 3$ biological replicates) below the gel. Inc: exon inclusion; skp: exon skipping. $^{**}P < 0.01$, $^{***}P < 0.001$, ns, not significant, *t*-test.

ESE sequences to identify potential binding motifs for SRSF6 and SRSF1. We predicted three potential binding motifs for SRSF6, TGCGGA (SRSF6–BM1), TGAGGA (SRSF6–BM2), and CACGGC (SRSF6–BM3), respectively (Fig. 4A). Similarly, we found three predicted motifs for SRSF1, AGGAGG (SRSF1–BM1), CACACG (SRSF1–BM2), and CTGCCGG (SRSF1–BM3), respectively (Fig. 4A). Among the predicted binding motifs, both SRSF6 and SRSF1 comprise one nonoverlapping binding motif (SRSF6–BM1 and SRSF1–BM3, respectively). In contrast, SRSF6–BM2 overlaps with SRSF1–BM1, and SRSF6–BM3 overlaps with SRSF1–BM2. We next asked whether the predicted binding motifs indeed bind to SRSF6 or/and SRSF1. For the convenience of analysis, we subdivided the entire ESE into four segments: ESE1 (harboring SRSF6–BM1, SRSF6–BM2, and SRSF1–BM1), ESE2, ESE3 (harboring SRSF6–BM3 and SRSF1–BM2), and ESE4 (harboring SRSF1-BM3) (Fig. 4A). Next, we examined the binding profiles of SRSF6 and SRSF1 in the RNA-affinity purified products from these RNA substrates by IB (Fig. 4B). We detected the binding affinity of both SRSF6 and SRSF1 for ESE1 and ESE3. ESE2 harbors no predicted binding sites for SRSF6 or SRSF1, and the lack of binding of these factors is in agreement with the prediction. Although ESE4 harbored a predicted binding site for SRSF1, we could not detect any binding affinity of SRSF1 for this motif. Taken together, we can conclude that RNA-segment spanning ESE1 and ESE3 possess true binding sites for both SRSF6 and SRSF1.

To illustrate whether the identified binding sites in ESE1 and ESE3 are functionally relevant to ESE activity, we introduced artificial mutations in these sites in pSPL3-human-*MUSK* minigene (pH-wt) in different combinations to weaken the predicted binding motif (Fig. 4C). Next, we assessed the splicing efficiency of these mutated minigenes in HeLa cells. Artificial mutations disrupting SRSF6–BM1 of ESE1 (ESE-mut1) caused a partial decrease in exon inclusion efficiency (Fig. 4D, lane 2 compared to lane 1). Similarly, mutations disrupting SRSF6–BM2 and SRSF1–BM1 of ESE1 (ESE-mut2) also caused a partial decrease in exon inclusion efficiency (Fig. 4D, lane 3 compared to lane 1). In contrast, mutations disrupting SRSF6–BM3 and SRSF1–BM2 of ESE3 (ESE-mut3) resulted in a significant decrease in exon inclusion activity (Fig. 4D, lane 4 compared to lane 1). These results suggest that ESE3 has a stronger activity than ESE1. In addition, mutations weakening all the binding sites of ESE1 and ESE3 completely abolished the exon inclusion activity. Taken together, we can enlist three functional splicing enhancing motifs (ESE motifs) in *MUSK* exon 10. ESE-motif1 (TGCGGA) and ESE-motif2 (TGAGGAGG) span ESE1, whereas ESE-motif3 (CACACGGC) spans ESE3 (Figs 4A and 5A).

Context-specific tethering of SRSF6 and SRSF1 can recapitulate their ESE activity.

Dissection of ESE motifs demonstrated a cooperative splicing regulation promoted by SRSF6 and SRSF1 through multiple ESE elements. We then tried to characterize the relative contribution of SRSF6 and SRSF1 in this coordination in the context of the identified ESE motifs. For this, we exploited bacteriophage MS2 coat protein-mediated artificial tethering experiments [9, 17, 33, 46]. We made three *MUSK* minigene reporters (pSPL3-*MUSK*-MS2-1/2/3), in which we substituted a specific ESE motif with an MS2-binding site, and the remaining two ESE motifs were inactivated by artificial mutations (Fig. 5A). These model reporters, therefore, possess compromised ESE motifs (as evident by the loss of exon inclusion, Fig. 5, lane 1 of panels C–E), which allows the opportunity to test the activity of an individual motif at a time by tethering an MS2-tagged *trans*-factor (Fig. 5B). Tethering of MS2-tagged SRSF1 (SRSF1–MS2) induced exon inclusion in pSPL3-*MUSK*-MS2-1 and pSPL3-*MUSK*-MS2-2 to a similar extent but not in pSPL3-*MUSK*-MS2-3 (Fig. 5C–E). These results suggest that SRSF1 can modulate the ESE-activity for ESE-motif1 and ESE-motif2 but not for ESE-motif3. In contrast, tethering of MS2-tagged SRSF6 (SRSF6–MS2) induced exon inclusion for all three reporters with variable extents, with the strongest effect in pSPL3-*MUSK*-MS2-3 (Fig. 5C–E). These results suggest that SRSF6 can modulate the ESE activity for all three motifs. Note that SRSF1 without an MS2-tag (SRSF1) could not induce exon inclusion in any of the reporters, suggesting no SRSF1 responsive binding sites elsewhere in the minigene. In contrast, SRSF6 without an MS2-tag (SRSF6) slightly induced exon inclusion in all three reporters, suggesting that SRSF6 might have other responsive elements elsewhere in the minigene. We confirmed that MS2 alone (MS2) and MS2-tagged factor hnRNP H (hnRNP H-MS2, unrelated to *MUSK* splicing) have no ESE activity for any of the reporters to exclude any possible experimental artifacts.

Differentiated muscle upregulates a wnt-sensitive MuSK isoform by downregulating splicing suppressors rather than enhancers

We previously showed that the inclusion of *MUSK* exon 10 is increased upon myogenic differentiation both in primary human myoblasts (SkMC) and immortalized human myogenic cells (Hu5/KD3) [9]. We also observed that the expression of splicing suppressors hnRNP C and YB-1 are also decreased upon myogenic differentiation. We, therefore, checked the expression profile of splicing enhancers SRSF6 and SRSF1 in myotubes differentiated from Hu5/KD3 (Fig. 6A). We found that expression of both SRSF6 and SRSF1 remained unchanged at both mRNA (Fig. 6B and C) and protein levels (Fig. 6D and E) during differentiation. Taken together, we can conclude that differentiated muscle reduces the expression of splicing suppressors hnRNP C and YB-1 while keeping the uniform expression of splicing enhancers to generate a Wnt-sensitive MuSK isoform (Fig. 6A–E).

Manipulation of MuSK isoform using antisense oligonucleotides

Having characterized the underlying regulation of *MUSK* isoform splicing, we next seek to develop a strategy for targeted manipulation of *MUSK* exon 10 AS, which could have a profound therapeutic impact in NMJ disorders. We employed antisense pharmacology. ASOs can bind to specific sequences in the target RNA and may inhibit the binding of splicing factors or generate steric hindrance to interfere with spliceosome assembly, resulting in differential AS outcomes [47–51]. We set out systematic ASO walks against *MUSK* pre-mRNA targeting ESS and ESE sequences in exon 10, as well as flanking splice sites (SS), 3′ SS, and 5′ SS (Fig. 7A). We designed affinity plus ASOs with 2′ modifications on the sugar moiety (locked nucleic acid bases) to prevent RNase H activation. These modifications allow high-affinity binding of ASOs and confer resistance to nuclease- and RNase H-mediated cleavage of the

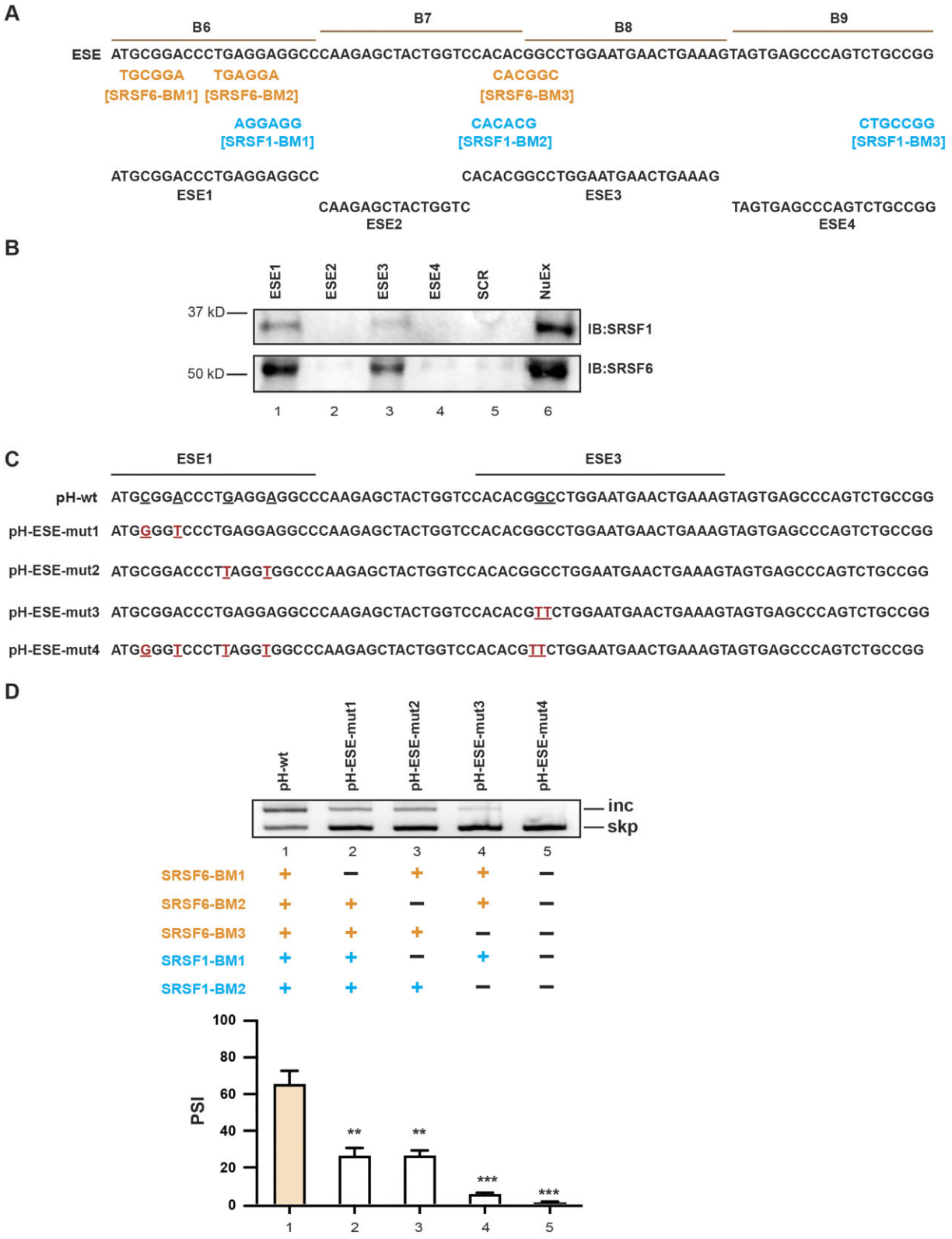

Figure 4. Decoding the functional splicing regulatory motifs spanning ESE of *MUSK* exon 10. (**A**) *MUSK* ESE sequences (spanning blocks B6–B9 in exon 10, see Fig. 2A). Predicted binding motifs of SRSF6 (orange) and SRSF1 (blue) are shown below. The entire ESE is subdivided into four parts (ESE1, ESE2, ESE3, and ESE4) to examine the binding of SRSF6 or/and SRSF1 in the predicted motifs, respectively. (**B**) RNA affinity-purified products from specified RNA probes are detected by IB with the indicated antibodies. SCR represents a scramble RNA probe used as a control. (**C**) Scanning mutagenesis to map the functional motifs in ESE. Artificial mutations introduced into ESE1 or/and ESE3 of pSPL3-human-*MUSK* minigene (pH-wt) are marked red and underlined. (**D**) RT-PCR of pSPL3-human-*MUSK* minigene (pH-wt) and four ESE-mutant minigenes (panel C) in HeLa cells. Plus and minus signs indicate the presence or absence of the predicted motif, respectively. Quantification of *MUSK* exon 10 inclusion (PSI) is shown by a bar graph (mean ± SD, $n = 3$ biological replicates) below the gel. Inc: exon inclusion; skp: exon skipping; NuEx: nuclear extract. $^{**}P < 0.01$, $^{***}P < 0.001$, ns: not significant, *t*-test.

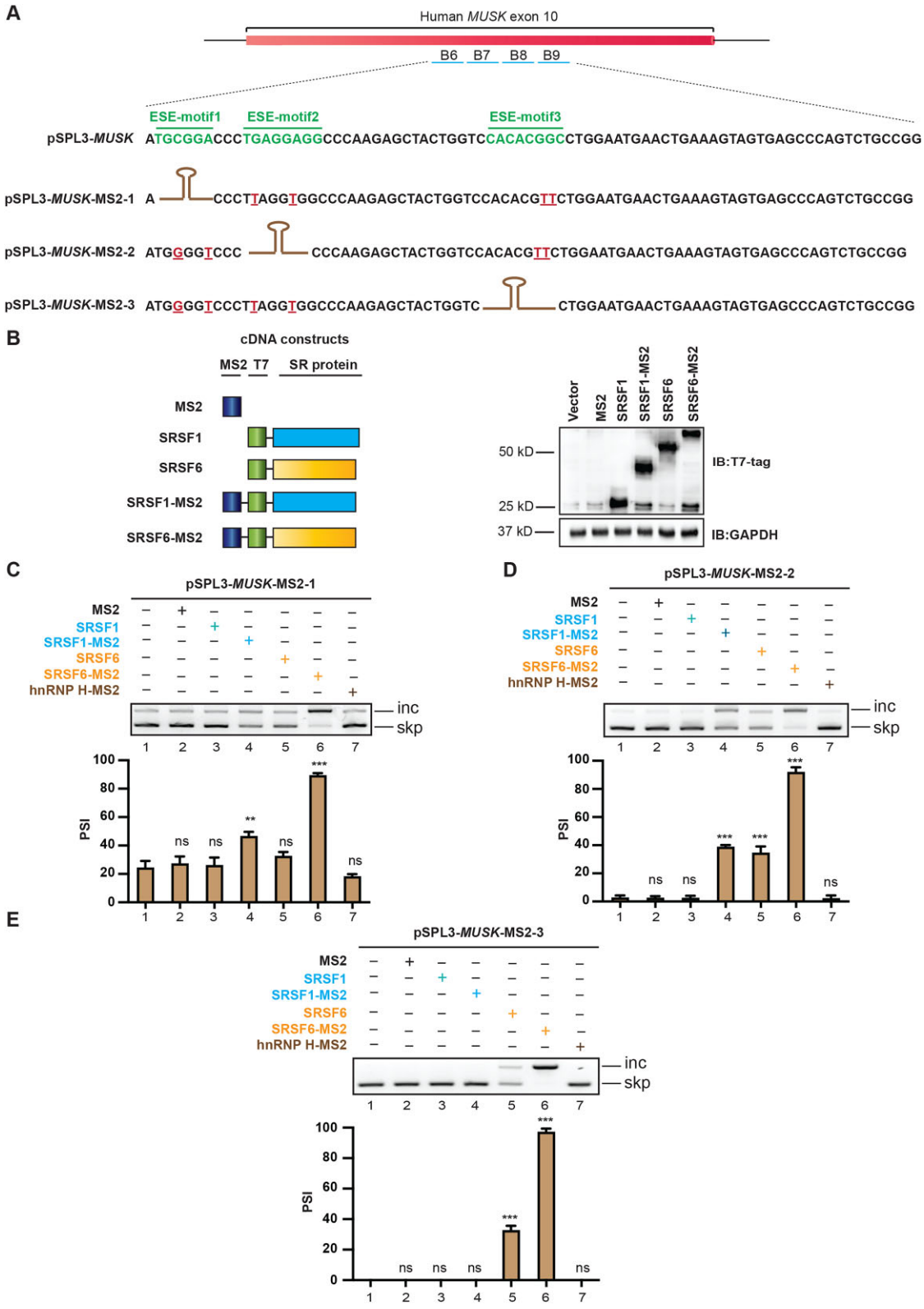

Figure 5. Examining ESE-activity of individual motifs by MS2-mediated tethering of SRSF6 or SRSF1. (**A**) Schematics of MS2-binding hairpin sequence inserted into ESE motifs (ESE-motif1, ESE-motif2, or ESE-motif3) in exon 10 of pSPL3-human-*MUSK* minigene (pH-wt) to recruit an MS2-tagged SRSF6 or SRSF1. To assess motif-specific splicing effect, one motif was replaced by an MS2-hairpin, and the remaining motifs were mutated to abrogate binding sites of SRSF6 or/and SRSF1. (**B**) Schematics of MS2-tagged cDNA constructs (left). IB with the indicated antibodies after MS2-tagged cDNA expression encoding human SRSF6 and SRSF1 in HeLa cells (right). MS2 cDNA (MS2) doesn't have a T7-tag. (**C**–**E**) RT-PCR of pSPL3-human-*MUSK-MS2-1/2/3* minigene in HeLa cells co-transfected with the indicated cDNAs. Plus and minus signs indicate the presence or absence of the indicated trans-factors, respectively. MS2-tagged hnRNP H is used as a negative control. Quantification of *MUSK* exon 10 inclusion (PSI) is shown by a bar graph (mean ± SD, $n = 3$ biological replicates) below the gel. Inc: exon inclusion; skp: exon skipping. $^{**}P < 0.01$; $^{***}P < 0.001$, ns: not significant, *t*-test.

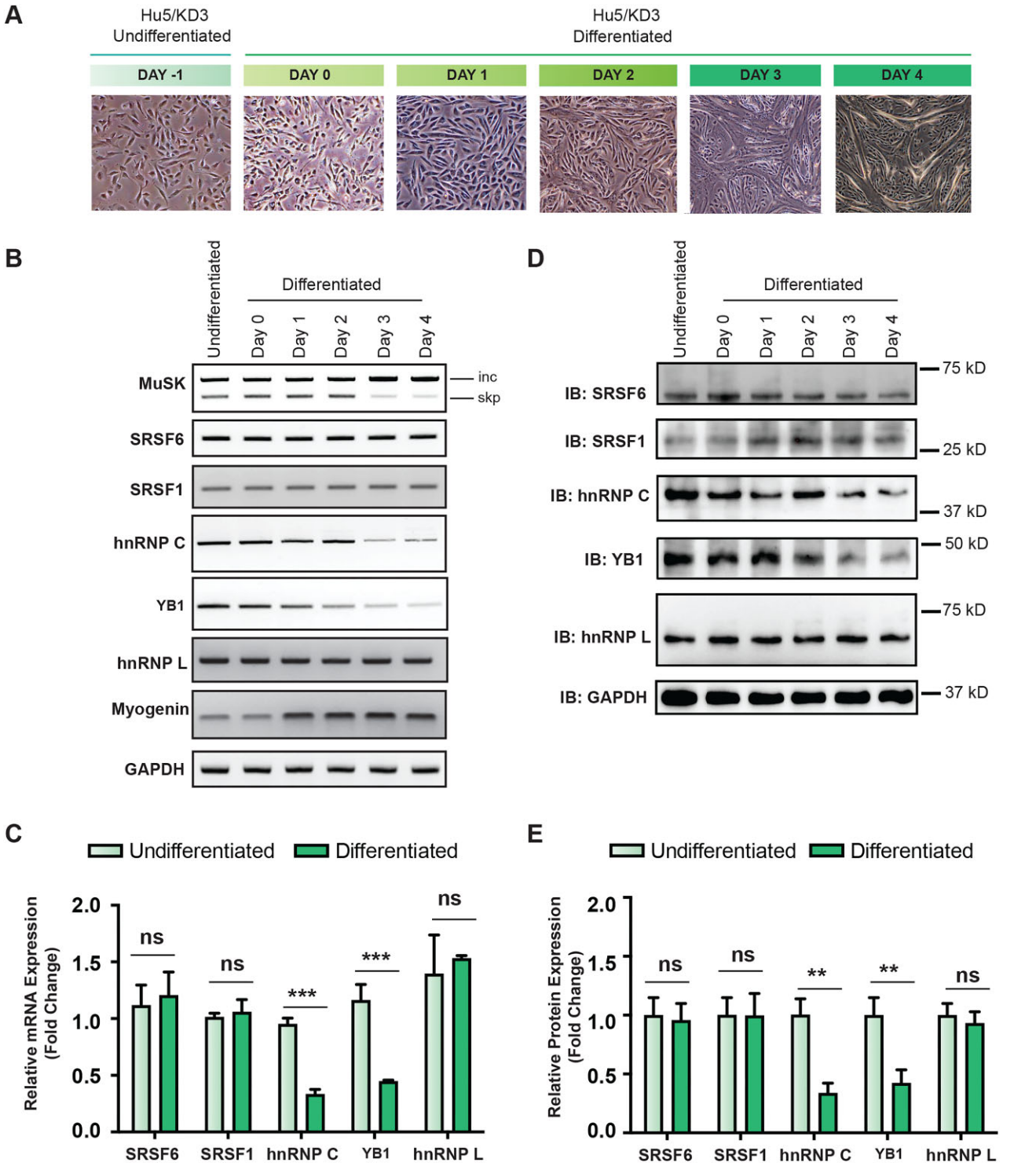

Figure 6. Expression of SRSF6 and SRSF1 upon myogenic differentiation. (**A**) Phase-contrast images showing a temporal profile of differentiation of human myogenic cell line (Hu5/KD3). (**B**) Time-course RT-PCR showing AS of endogenous *MUSK* exon 10 and endogenous expression of its splicing enhancers (SRSF6 and SRSF1) and splicing suppressors (hnRNP C, YB-1, and hnRNP L) at different differentiation days of Hu5/KD3. Expressions of myogenin and GAPDH are shown as internal controls (**C**) Densitometric quantification of relative mRNA expression levels of splicing enhancers and suppressors in undifferentiated (Day -1) and differentiated (Day 4) Hu5/KD3 as described in panel (B). GAPDH is used as the control for normalization. Bar graph (mean ± SD, $n = 3$ biological replicates). (**D**) Time-course IB at different differentiation days of Hu5/KD3 with indicated antibodies. (**E**) Densitometric quantification of relative protein expression levels of splicing enhancers and suppressors in undifferentiated (Day -1) and differentiated (Day 4) Hu5/KD3 as described in panel (D). GAPDH is used as the control for normalization. Bar graph (mean ± SD, $n = 3$ biological replicates). Inc: exon inclusion; skp: exon skipping. $^{**}P < 0.01$; $^{***}P < 0.001$, ns: not significant, *t*-test.

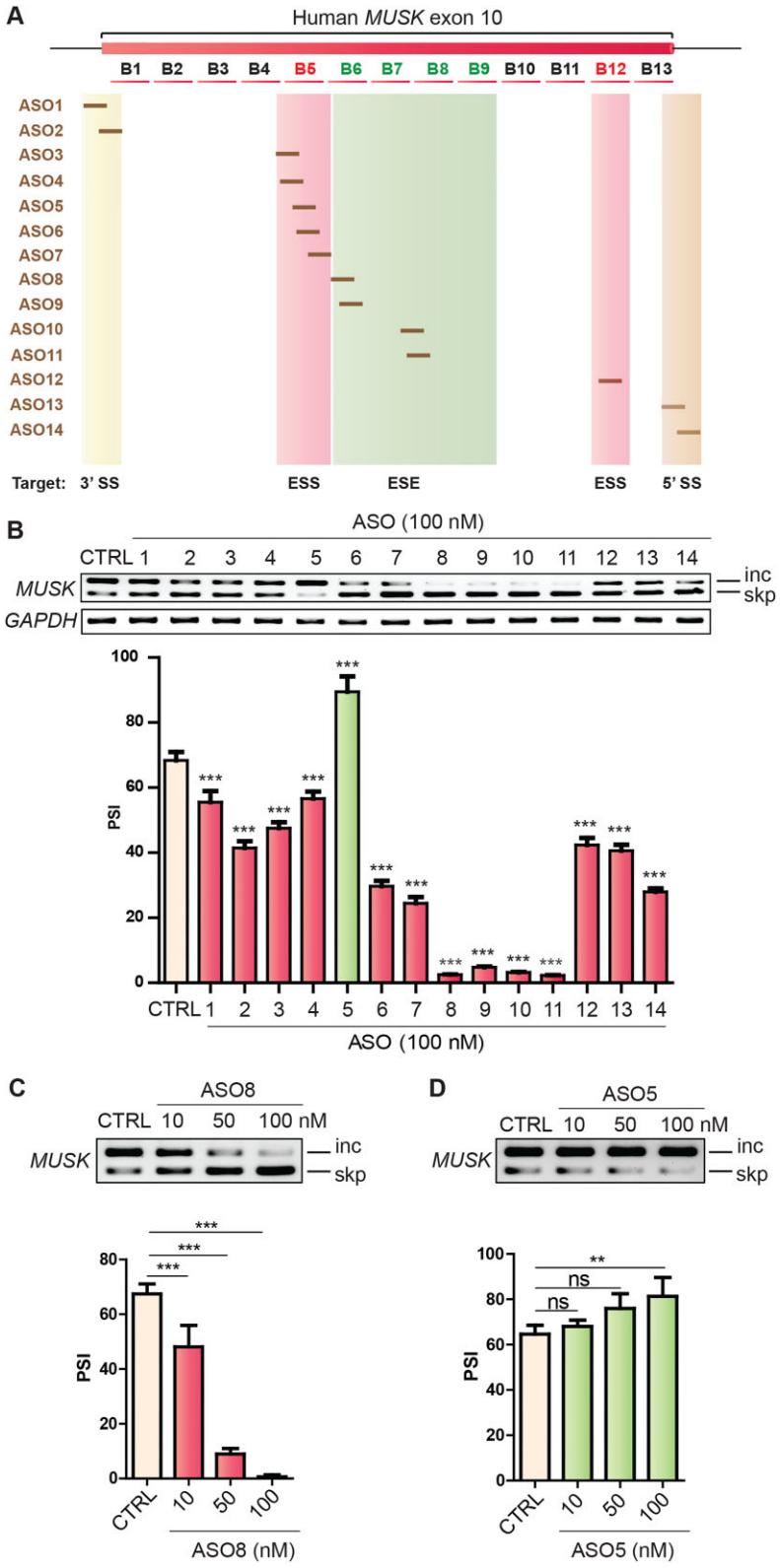

Figure 7. Manipulation of *MUSK* isoforms using ASOs. (**A**) Schematic of ASO walks spanning *MUSK* exon 10 and flanking splice sites. (**B**) RT-PCR of pSPL3-human-*MUSK* minigene (pH-wt) in HeLa cells cotransfected with the indicated ASOs for 48 h. Quantification of *MUSK* exon 10 inclusion (PSI) is shown by a bar graph (mean ± SD, $n = 3$ biological replicates) below the gel. (**C** and **D**) RT-PCR of pSPL3-human-*MUSK* minigene (pH-wt) in HeLa cells cotransfected with the indicated ASOs at increasing concentrations for 48 h. Quantification of *MUSK* exon 10 inclusion (PSI) is shown by a bar graph (mean ± SD, $n = 3$ biological replicates) below the gel. CTRL: mock treatment control with no ASO; Inc: exon inclusion; skp: exon skipping. $^{**}P < 0.01$, $^{***}P < 0.001$, ns: not significant, *t*-test.

target RNA [47, 48, 51–53]. We designed 14 ASOs: ASO1–ASO2 targeting splice site upstream of exon 10 (3′ splice site), ASO3–ASO7 targeting ESS (block 5), ASO8–ASO11 targeting ESE, ASO12 targeting ESS (block 12), and ASO13–ASO14 targeting splice site downstream of exon 10 (5′ splice site) (Fig. 7A). We tested these ASOs in HeLa cells co-transfected with the pSPL3-human-*MUSK* minigene (pH-wt). As a control, we employed a mock treatment with no ASO (CTRL). We also tested a nontargeting ASO (NT-ASO, targeting an unrelated gene *EZH2*) (Supplementary Fig. S2). RT-PCR was conducted to detect both exon-included (inc) and exon-skipped (skp) products (Fig. 7B). The results identified ASOs with differential exon-skipping efficiencies: ASOs with strong exon-skipping activities (ASO8, ASO9, ASO10, and ASO11); ASOs with moderate exon-skipping activities (ASO6, ASO7, and ASO14); and ASOs with low exon-skipping activities (ASO1, ASO2, ASO3, ASO4, ASO12, and ASO13) (Fig. 7B). Among 14 ASOs, only ASO5 showed exon-inclusion activity (Fig. 7A and B).

To determine whether the extent of ASO-mediated manipulation of *MUSK* mRNA isoforms can be titrated, one exon-skipping-promoting candidate (ASO8) (Fig. 7C) and one exon-inclusion-promoting candidate (ASO5) (Fig. 7D) were tested further for dose-dependent response experiments. To this end, cells were treated with ASOs at increasing concentrations (10, 50, and 100 nM). As we expected, ASO8 showed dose-dependent effects on exon-skipping, whereas ASO5 showed dose-dependent effects on exon-inclusion.

Discussion

In this study, we precisely characterized the ESE *cis*-elements of *MUSK* exon 10 and determined the functional motifs in the ESE. We also identified cognate *trans*-factors and demonstrated that SRSF6 and SRSF1 coordinately enhance exon inclusion through multiple functional motifs in the ESE. Between the two factors, SRSF6 potentially exerts a stronger regulatory effect, whereas SRSF1 cooperates with an additive effect. In our previous report, we tested the relative binding affinity of SRSF1 for several degenerative motifs [46]. We found that GGAGG possesses a high binding affinity for SRSF1, GGTGG, and GGCGG possess moderate binding affinity, and GGGGG possesses no binding affinity. Among the ESE motifs of *MUSK* exon 10 (ESE-motif1: TGCGGAC, ESE-motif2: TGAGGAGG, ESE-motif3: CACGGCCT), only one high affinity-binding motif GGAGG is present in ESE-motif2 (TGAGGAGG). Indeed, in the binding study, we detected considerable binding of SRSF1 only for the ESE1 probe harboring ESE-motif1 and ESE-motif2 (Fig. 4B). In contrast, the relative binding affinity for different degenerative motifs of SRSF6 has not been dissected concisely to date. However, we noticed strong binding of SRSF6 for both ESE1 and ESE3, which suggests that these motifs possess strong binding affinity for SRSF6. Inactivating native binding motif(s) and artificial recruitment of each splicing factor by MS2-mediated tethering again demonstrated a stronger effect of SRSF6 compared to SRSF1 (Fig. 5C–E). One critical observation came out in these experiments that SRSF6 has additional responsive motif(s) besides those in exon 10, as SRSF6 without an MS2-tag slightly induced exon inclusion in all three MS2 reporters (Fig. 5C–E). In contrast, SRSF1 responsive elements are only limited to exon 10. The presence of several high-affinity binding motifs and additional motif(s) outside of exon 10 can reasonably explain the stronger splicing-enhancing effect of SRSF6 than SRSF1.

We previously reported the underlying regulation of skipping of *MUSK* exon 10 in humans, which is absent in mice. We identified a unique ESS in human *MUSK* exon 10, which promotes exon skipping by the complex and coordinated interplay of *trans*-acting factors hnRNP C, YB-1, and hnRNP L. The present study, along with our previous study, enabled us to decipher the complete underlying regulation of *MUSK* exon 10 splicing associated with an important domain essential for Wnt-mediated AChRs clustering at NMJ. Analysis of *MUSK* splicing in the course of myogenic differentiation and evaluation of the expression profile of splicing regulators led us to reveal an important physiological control of myogenesis. We found that differentiated muscle reduces the expression of splicing suppressors (hnRNP C and YB-1) but not enhancers to generate a Wnt-sensitive MuSK isoform to augment Wnt-mediated AChRs clustering at NMJ. Interestingly, it was reported that the expression levels of hnRNP C, YB-1, and even hnRNP L are also downregulated in differentiated conditions in mouse myoblast cells (C2C12) [54, 55]. An interesting question arises here: Why do differentiated muscle cells decrease the expression of splicing suppressors rather than increasing splicing enhancers? *SRSF1* functions as a proto-oncogene when it is overexpressed [22–24]. SRSF1 was reported to be overexpressed in tumors from breast, small intestine, colon, kidney, thyroid, lung, liver, and pancreas [22–24]. On the other hand, SRSF6 was also reported to function as an oncoprotein to regulate the proliferation and survival of lung and colon cancers [29]. These suggest that the increased level of SRSF1 or SRSF6 could be detrimental to cells. In contrast, YB-1 is reported as a negative regulator of C2C12 myoblast differentiation [55]. YB-1 cooperatively interacts with MSX1, which inhibits the expression of MyoD by binding to the core enhancer region (CER) of the MyoD promoter [55]. Therefore, the reduction of YB-1 expression in the course of differentiation is also physiologically relevant to facilitate myogenic differentiation. Therefore, to achieve beneficial expression of the Wnt-sensitive MuSK isoform at NMJ, humans may have acquired ESS in the course of evolution to selectively skip exon 10 by utilizing spatiotemporally regulated expressions of splicing suppressors, which is absent in mice.

AS plays an unprecedented role in controlling gene expression at NMJ, and a lot of reports showed that aberrant regulation of splicing often compromises the safety margin of neuromuscular signal transmission and gives rise to pathological clinical consequences at NMJ [33, 46, 56–60]. Therefore, decoding splicing regulation in molecules, which constitute the molecular architecture of NMJ, could have profound clinical significance. For example, we dissected splicing regulation in *CHRNA1* encoding AChRs alpha subunit, where we showed that hnRNP L, PTB, and hnRNP H promote skipping of a nonfunctional exon P3A [33, 61]. Investigation of two pathogenic splicing mutations in two patients with congenital myasthenic syndrome (CMS) allowed us to demonstrate that IVS3-8G > A disrupts binding of hnRNP H in one patient [61], and P3A23′G > A disrupts binding of hnRNP L in another patient [33]. In both cases, disruption of either hnRNP H or hnRNP L causes aberrant and exclusive inclusion of exon P3A, which subsequently disables the expression of AChRs at the patient end-plate. In *COLQ*, SRSF1 promotes the inclusion of a constitutive exon 16 of *COLQ*

[46]. A pathogenic variant p.E415G disrupting the binding of SRSF1 triggers aberrant exon skipping and subsequently causes end-plate acetylcholinesterase deficiency at the patient end-plate [46]. Splicing dissection of *MUSK* exon 10 in this study and our previous study [9] provide ample opportunity to screen potential pathogenic mutations causing splicing defects in *MUSK* associated with NMJ disorders. However, to the best of our knowledge, no mutations have been reported in the identified splicing *cis*-elements of *MUSK* to date.

Therapeutic approaches correcting splicing errors have been successfully transformed to the clinic for several genetic disorders [47–51, 62]. ASOs-mediated splice-switching has been developed as an effective targeted approach in recent times. For example, the ASO drug Nusinersen (Spinraza) corrects aberrant splicing of *SMN2*, which appeared as an effective approved treatment for a neurological disorder, spinal muscular atrophy (SMA) [48, 62]. Nusinersen binds to a splicing regulatory intronic region flanking exon 7 in *SMN2*. This binding enhances the inclusion of exon 7 in the mRNA, which encodes a functional full-length protein. The full-length protein is normally lacking in SMA patients due to homozygous mutations or deletions of the *SMN1* gene [47, 48, 62]. However, the splice-switching strategy has not been successfully employed in clinical development for CMS and related NMJ disorders. As a proof-of-concept, to manipulate AS at NMJ, we developed ASOs targeting the splicing regulatory elements (ESSs and ESEs) in *MUSK* identified in our studies, as well as flanking splice sites (5′ splice site and 3′ splice site). To our expectation, the ASOs (ASO8, ASO9, ASO10, and ASO11) spanning the identified functional motifs in the ESE of *MUSK* exon 10 exerted efficient exon-skipping, likely due to inhibiting the binding of splicing enhancers (SRSF6 and SRSF1) (Fig. 7). Similarly, the ASO (ASO5) spanning one of the identified ESSs of *MUSK* exon 10 (ESS5) exerted efficient exon-inclusion activity, likely due to blocking the binding of splicing suppressors (hnRNP C, YB-1, and hnRNP L) (Fig. 7). These data suggest that understanding and characterizing splicing regulatory motifs in genes associated with NMJ could strongly help in developing efficient, successful therapeutic strategies to correct splicing errors in patients with CMS and related NMJ disorders. Therefore, our studies could represent a modality for the discovery and development of a mechanism-based systematic strategy to manipulate pathogenic AS for therapeutic intervention in CMS and related NMJ disorders.

Acknowledgements

We are grateful to Naohiro Hashimoto (National Center for Geriatrics and Gerontology) for sharing Hu5/KD3 cells, Adrian Krainer (Cold Spring Harbor Laboratory) for sharing SRSF1 and SRSF6 cDNA constructs and anti-T7-tag antibody, Kentaro Taki (Nagoya University) for technical assistance on the mass spectrometry analysis, and Akio Masuda (Nagoya University) for critical review of the manuscript and valuable advice.

Author contributions: M.A.R. and K.O. conceived the project. F.N., M.A.R., and K.O. designed experiments. F.N., P.N., M.R.I., S.A.H., M.M.H., and M.A.R. performed experiments. F.N. and M.A.R. wrote the initial draft of the manuscript with inputs from all authors. M.A.R. and K.O. revised the manuscript. All authors approved the final version of the manuscript.

Supplementary data

Supplementary data is available at NAR Molecular Medicine online.

Conflict of interest

None declared.

Funding

We acknowledge support from the National Institute of General Medical Sciences (NIGMS) of the National Institutes of Health (R35GM154991 to M.A.R.), the Winthrop P. Rockefeller Cancer Institute to M.A.R.; Grants-in-Aid from the Japan Society for the Promotion of Science (JP23H02794 to K.O., JP23K18273 to K.O.); the Ministry of Health, Labour, and Welfare of Japan (23FC1014 to K.O.); and the Intramural Research Grant for Neurological and Psychiatric Disorders of NCNP (5-6 to KO).

Data availability

The data underlying this article are available in this article and its online Supplementary Data.

References

1. Licatalosi DD, Darnell RB. Splicing regulation in neurologic disease. *Neuron* 2006;**52**:93–101. https://doi.org/10.1016/j.neuron.2006.09.017
2. Cooper TA, Wan L, Dreyfuss G. RNA and disease. *Cell* 2009;**136**:777–93. https://doi.org/10.1016/j.cell.2009.02.011
3. Pan Q, Shai O, Lee LJ *et al.* Deep surveying of alternative splicing complexity in the human transcriptome by high-throughput sequencing. *Nat Genet* 2008;**40**:1413–5. https://doi.org/10.1038/ng.259
4. Rahman MA, Krainer AR, Abdel-Wahab O. SnapShot: splicing alterations in cancer. *Cell* 2020;**180**:208. https://doi.org/10.1016/j.cell.2019.12.011
5. Bradley RK, Anczuków O. RNA splicing dysregulation and the hallmarks of cancer. *Nat Rev Cancer* 2023;**23**:135–55. https://doi.org/10.1038/s41568-022-00541-7
6. Stiegler AL, Burden SJ, Hubbard SR. Crystal structure of the frizzled-like cysteine-rich domain of the receptor tyrosine kinase MuSK. *J Mol Biol* 2009;**393**:1–9. https://doi.org/10.1016/j.jmb.2009.07.091
7. Xu YK, Nusse R. The frizzled CRD domain is conserved in diverse proteins including several receptor tyrosine kinases. *Curr Biol* 1998;**8**:R405–6. https://doi.org/10.1016/S0960-9822(98)70262-3
8. Masiakowski P, Yancopoulos GD. The wnt receptor CRD domain is also found in MuSK and related orphan receptor tyrosine kinases. *Curr Biol* 1998;**8**:R407. https://doi.org/10.1016/S0960-9822(98)70263-5
9. Nasrin F, Rahman MA, Masuda A *et al.* HnRNP C, YB-1 and hnRNP L coordinately enhance skipping of human musk exon 10 to generate a wnt-insensitive musk isoform. *Sci Rep* 2014;**4**:6841. https://doi.org/10.1038/srep06841
10. Zhang W, Coldefy A-S, Hubbard SR *et al.* Agrin binds to the N-terminal region of Lrp4 protein and stimulates association between Lrp4 and the first immunoglobulin-like domain in muscle-specific kinase (MuSK). *J Biol Chem* 2011;**286**:40624–30. https://doi.org/10.1074/jbc.M111.279307
11. Valenzuela DM, Stitt TN, DiStefano PS *et al.* Receptor tyrosine kinase specific for the skeletal muscle lineage: expression in embryonic muscle, at the neuromuscular junction, and after injury.

Neuron 1995;**15**:573–84. https://doi.org/10.1016/0896-6273(95)90146-9
12. Jennings CG, Dyer SM, Burden SJ. Muscle-specific trk-related receptor with a kringle domain defines a distinct class of receptor tyrosine kinases. *Proc Natl Acad Sci USA* 1993;**90**:2895–9. https://doi.org/10.1073/pnas.90.7.2895
13. Manley JL, Krainer AR. A rational nomenclature for serine/arginine-rich protein splicing factors (SR proteins): table 1. *Genes Dev* 2010;**24**:1073–4. https://doi.org/10.1101/gad.1934910
14. Pandit S, Zhou Y, Shiue L *et al.* Genome-wide analysis reveals SR protein cooperation and competition in regulated splicing. *Mol Cell* 2013;**50**:223–35. https://doi.org/10.1016/j.molcel.2013.03.001
15. Zhang Z, Krainer AR. Involvement of SR proteins in mRNA surveillance. *Mol Cell* 2004;**16**:597–607. https://doi.org/10.1016/j.molcel.2004.10.031
16. Aznarez I, Nomakuchi TT, Tetenbaum-Novatt J *et al.* Mechanism of nonsense-mediated mRNA decay stimulation by splicing factor SRSF1. *Cell Rep* 2018;**23**:2186–98. https://doi.org/10.1016/j.celrep.2018.04.039
17. Rahman MA, Lin K-T, Bradley RK *et al.* Recurrent SRSF2 mutations in MDS affect both splicing and NMD. *Genes Dev* 2020;**34**:413–27. https://doi.org/10.1101/gad.332270.119
18. Müller-McNicoll M, Botti V, de Jesus Domingues AM *et al.* SR proteins are NXF1 adaptors that link alternative RNA processing to mRNA export. *Genes Dev* 2016;**30**:553–66. https://doi.org/10.1101/gad.276477.115
19. Huang Y, Yario TA, Steitz JA. A molecular link between SR protein dephosphorylation and mRNA export. *Proc Natl Acad Sci USA* 2004;**101**:9666–70. https://doi.org/10.1073/pnas.0403533101
20. Huang Y, Gattoni R, Stévenin J *et al.* SR splicing factors serve as adapter proteins for TAP-dependent mRNA export. *Mol Cell* 2003;**11**:837–43. https://doi.org/10.1016/S1097-2765(03)00089-3
21. Sun S, Zhang Z, Sinha R *et al.* SF2/ASF autoregulation involves multiple layers of post-transcriptional and translational control. *Nat Struct Mol Biol* 2010;**17**:306–12. https://doi.org/10.1038/nsmb.1750
22. Karni R, de Stanchina E, Lowe SW *et al.* The gene encoding the splicing factor SF2/ASF is a proto-oncogene. *Nat Struct Mol Biol* 2007;**14**:185–93. https://doi.org/10.1038/nsmb1209
23. Anczuków O, Rosenberg AZ, Akerman M *et al.* The splicing factor SRSF1 regulates apoptosis and proliferation to promote mammary epithelial cell transformation. *Nat Struct Mol Biol* 2012;**19**:220–8. https://doi.org/10.1038/nsmb.2207
24. Leclair NK, Brugiolo M, Urbanski L *et al.* Poison exon splicing regulates a coordinated network of SR protein expression during differentiation and tumorigenesis. *Mol Cell* 2020;**80**:648–65. https://doi.org/10.1016/j.molcel.2020.10.019
25. Yin X, Jin N, Gu J *et al.* Dual-specificity tyrosine phosphorylation-regulated kinase 1A (Dyrk1A) modulates serine/arginine-rich protein 55 (SRp55)-promoted tau exon 10 inclusion. *J Biol Chem* 2012;**287**:30497–506. https://doi.org/10.1074/jbc.M112.355412
26. Juan-Mateu J, Alvelos MI, Turatsinze J-V *et al.* SRp55 regulates a splicing network that controls human pancreatic β-cell function and survival. *Diabetes* 2018;**67**:423–36. https://doi.org/10.2337/db17-0736
27. Swanson CM, Sherer NM, Malim MH. SRp40 and SRp55 promote the translation of unspliced human immunodeficiency virus type 1 RNA. *J Virol* 2010;**84**:6748–59. https://doi.org/10.1128/JVI.02526-09
28. Jensen MA, Wilkinson JE, Krainer AR. Splicing factor SRSF6 promotes hyperplasia of sensitized skin. *Nat Struct Mol Biol* 2014;**21**:189–97. https://doi.org/10.1038/nsmb.2756
29. Cohen-Eliav M, Golan-Gerstl R, Siegfried Z *et al.* The splicing factor SRSF6 is amplified and is an oncoprotein in lung and colon cancers. *J Pathol* 2013;**229**:630–9. https://doi.org/10.1002/path.4129
30. Hashimoto N, Kiyono T, Wada MR *et al.* Immortalization of human myogenic progenitor cell clone retaining multipotentiality. *Biochem Biophys Res Commun* 2006;**348**:1383–8. https://doi.org/10.1016/j.bbrc.2006.08.006
31. Wada MR, Inagawa-Ogashiwa M, Shimizu S *et al.* Generation of different fates from multipotent muscle stem cells. *Development* 2002;**129**:2987–95. https://doi.org/10.1242/dev.129.12.2987
32. Shiomi K, Kiyono T, Okamura K *et al.* CDK4 and cyclin D1 allow human myogenic cells to recapture growth property without compromising differentiation potential. *Gene Ther* 2011;**18**:857–66. https://doi.org/10.1038/gt.2011.44
33. Rahman MA, Masuda A, Ohe K *et al.* HnRNP L and hnRNP LL antagonistically modulate PTB-mediated splicing suppression of CHRNA1 pre-mRNA. *Sci Rep* 2013;**3**:2931. https://doi.org/10.1038/srep02931
34. Cáceres JF, Misteli T, Screaton GR *et al.* Role of the modular domains of SR proteins in subnuclear localization and alternative splicing specificity. *J Cell Biol* 1997;**138**:225–38. https://doi.org/10.1083/jcb.138.2.225
35. Schaal TD, Maniatis T. Multiple distinct splicing enhancers in the protein-coding sequences of a constitutively spliced pre-mRNA. *Mol Cell Biol* 1999;**19**:261–73. https://doi.org/10.1128/MCB.19.1.261
36. Tong A, Nguyen J, Lynch KW. Differential expression of CD45 isoforms is controlled by the combined activity of basal and inducible splicing-regulatory elements in each of the variable exons. *J Biol Chem* 2005;**280**:38297–304. https://doi.org/10.1074/jbc.M508123200
37. Black DL. Mechanisms of alternative pre-messenger RNA splicing. *Annu Rev Biochem* 2003;**72**:291–336. https://doi.org/10.1146/annurev.biochem.72.121801.161720
38. Cartegni L, Wang J, Zhu Z *et al.* ESEfinder: a web resource to identify exonic splicing enhancers. *Nucleic Acids Res* 2003;**31**:3568–71. https://doi.org/10.1093/nar/gkg616
39. Smith PJ, Zhang C, Wang J *et al.* An increased specificity score matrix for the prediction of SF2/ASF-specific exonic splicing enhancers. *Hum Mol Genet* 2006;**15**:2490–508. https://doi.org/10.1093/hmg/ddl171
40. Fairbrother WG, Yeo GW, Yeh R *et al.* RESCUE-ESE identifies candidate exonic splicing enhancers in vertebrate exons. *Nucleic Acids Res* 2004;**32**:W187–90. https://doi.org/10.1093/nar/gkh393
41. Liu H-X, Zhang M, Krainer AR. Identification of functional exonic splicing enhancer motifs recognized by individual SR proteins. *Genes Dev* 1998;**12**:1998–2012. https://doi.org/10.1101/gad.12.13.1998
42. Schaal TD, Maniatis T. Selection and characterization of pre-mRNA splicing enhancers: identification of novel SR protein-specific enhancer sequences. *Mol Cell Biol* 1999;**19**:1705–19. https://doi.org/10.1128/MCB.19.3.1705
43. Sanford JR, Coutinho P, Hackett JA *et al.* Identification of nuclear and cytoplasmic mRNA targets for the shuttling protein SF2/ASF. *PLoS One* 2008;**3**:e3369. https://doi.org/10.1371/journal.pone.0003369
44. Anczuków O, Akerman M, Cléry A *et al.* SRSF1-regulated alternative splicing in breast cancer. *Mol Cell* 2015;**60**:105–17. https://doi.org/10.1016/j.molcel.2015.09.005
45. Anczuków O, Krainer AR. Splicing-factor alterations in cancers. *RNA* 2016;**22**:1285–301. https://doi.org/10.1261/rna.057919.116
46. Rahman MA, Azuma Y, Nasrin F *et al.* SRSF1 and hnRNP H antagonistically regulate splicing of COLQ exon 16 in a congenital myasthenic syndrome. *Sci Rep* 2015;**5**:13208. https://doi.org/10.1038/srep13208
47. Havens MA, Hastings ML. Splice-switching antisense oligonucleotides as therapeutic drugs. *Nucleic Acids Res* 2016;**44**:6549–63. https://doi.org/10.1093/nar/gkw533

48. Rigo F, Hua Y, Krainer AR *et al.* Antisense-based therapy for the treatment of spinal muscular atrophy. *J Cell Biol* 2012;**199**:21–5. https://doi.org/10.1083/jcb.201207087
49. Nomakuchi TT, Rigo F, Aznarez I *et al.* Antisense oligonucleotide–directed inhibition of nonsense-mediated mRNA decay. *Nat Biotechnol* 2016;**34**:164–6. https://doi.org/10.1038/nbt.3427
50. Ma WK, Voss DM, Scharner J *et al.* ASO-based PKM splice-switching therapy inhibits hepatocellular carcinoma growth. *Cancer Res* 2022;**82**:900–15. https://doi.org/10.1158/0008-5472.CAN-20-0948
51. Lim KH, Han Z, Jeon HY *et al.* Antisense oligonucleotide modulation of non-productive alternative splicing upregulates gene expression. *Nat Commun* 2020;**11**:3501. https://doi.org/10.1038/s41467-020-17093-9
52. Prakash T, Bhat B. 2′-Modified oligonucleotides for antisense therapeutics. *CTMC* 2007;**7**:641–9. https://doi.org/10.2174/156802607780487713
53. Kurreck J, Wyszko E, Gillen C *et al.* Design of antisense oligonucleotides stabilized by locked nucleic acids. *Nucleic Acids Res* 2002;**30**:1911–8. https://doi.org/10.1093/nar/30.9.1911
54. Bland CS, Wang ET, Vu A *et al.* Global regulation of alternative splicing during myogenic differentiation. *Nucleic Acids Res* 2010;**38**:7651–64. https://doi.org/10.1093/nar/gkq614
55. Song YJ, Lee H. YB1/p32, a nuclear Y-box binding protein 1, is a novel regulator of myoblast differentiation that interacts with Msx1 homeoprotein. *Exp Cell Res* 2010;**316**:517–29. https://doi.org/10.1016/j.yexcr.2009.12.003
56. Ohno K, Rahman MA, Nazim M *et al.* Splicing regulation and dysregulation of cholinergic genes expressed at the neuromuscular junction. *J Neurochem* 2017;**142**:64–72. https://doi.org/10.1111/jnc.13954
57. Engel AG, Ohno K, Sine SM. Sleuthing molecular targets for neurological diseases at the neuromuscular junction. *Nat Rev Neurosci* 2003;**4**:339–52. https://doi.org/10.1038/nrn1101
58. Rahman MA, Ohno K. Splicing aberrations in congenital myasthenic syndromes. *J Invest Genomics* 2015;**2**:111–8.
59. Shibata A, Okuno T, Rahman MA *et al.* IntSplice: prediction of the splicing consequences of intronic single-nucleotide variations in the human genome. *J Hum Genet* 2016;**61**:633–40. https://doi.org/10.1038/jhg.2016.23
60. Gao Y, Lin K-T, Jiang T *et al.* Systematic characterization of short intronic splicing-regulatory elements in SMN2 pre-mRNA. *Nucleic Acids Res* 2022;**50**:731–49. https://doi.org/10.1093/nar/gkab1280
61. Masuda A, Shen X-M, Ito M *et al.* HnRNP H enhances skipping of a nonfunctional exon P3A in CHRNA1 and a mutation disrupting its binding causes congenital myasthenic syndrome. *Hum Mol Genet* 2008;**17**:4022–35. https://doi.org/10.1093/hmg/ddn305
62. Hua Y, Vickers TA, Okunola HL *et al.* Antisense masking of an hnRNP A1/A2 intronic splicing silencer corrects SMN2 splicing in transgenic mice. *Am Hum Genet* 2008;**82**:834–48. https://doi.org/10.1016/j.ajhg.2008.01.014

Received: January 2, 2025. **Revised:** March 7, 2025. **Editorial Decision:** March 17, 2025. **Accepted:** March 18, 2025